The rheology of multiwalled carbon nanotube and carbon black suspensions

Kathryn M Yearsley, Malcolm R Mackley, Francisco Chinesta, Adrien Leygue

▶ **To cite this version:**

Kathryn M Yearsley, Malcolm R Mackley, Francisco Chinesta, Adrien Leygue. The rheology of multiwalled carbon nanotube and carbon black suspensions. Journal of Rheology, 2012, 56 (6), pp.1465-1490. 10.1122/1.4751871 . hal-04325491

HAL Id: hal-04325491
https://hal.science/hal-04325491v1

Submitted on 6 Dec 2023

HAL is a multi-disciplinary open access archive for the deposit and dissemination of scientific research documents, whether they are published or not. The documents may come from teaching and research institutions in France or abroad, or from public or private research centers.

L'archive ouverte pluridisciplinaire **HAL**, est destinée au dépôt et à la diffusion de documents scientifiques de niveau recherche, publiés ou non, émanant des établissements d'enseignement et de recherche français ou étrangers, des laboratoires publics ou privés.

Copyright

JOURNAL OF RHEOLOGY

The rheology of multiwalled carbon nanotube and carbon black suspensions

Kathryn M. Yearsley, Malcolm R. Mackley, Francisco Chinesta, and Adrien Leygue

Citation: J. Rheol. **56**, 1465 (2012); doi: 10.1122/1.4751871
View online: http://dx.doi.org/10.1122/1.4751871
View Table of Contents: http://www.journalofrheology.org/resource/1/JORHD2/v56/i6
Published by the The Society of Rheology

Additional information on J. Rheol.

Journal Homepage: http://www.journalofrheology.org/
Journal Information: http://www.journalofrheology.org/about
Top downloads: http://www.journalofrheology.org/most_downloaded
Information for Authors: http://www.journalofrheology.org/author_information

ADVERTISEMENT

Downloaded 29 Nov 2012 to 81.132.17.87. Redistribution subject to SOR license or copyright; see http://www.journalofrheology.org/masthead

The rheology of multiwalled carbon nanotube and carbon black suspensions

Kathryn M. Yearsley[a] and Malcolm R. Mackley

Department of Chemical Engineering and Biotechnology, University of Cambridge, Cambridge CB2 3RA, United Kingdom

Francisco Chinesta and Adrien Leygue

Ecole Centrale of Nantes, 1 Rue de la Noe, 44300 Nantes, France

(Received 17 January 2012; final revision received 18 August 2012; published 17 September 2012)

Synopsis

This paper is concerned with a direct experimental and modeling comparison of the rheology of carbon black (CB) and multiwalled carbon nanotube (CNT) suspensions within a Newtonian epoxy matrix. Experimental observations of the effect of shear on CB and CNT microstructure are reported for a range of CB and CNT suspension concentrations. Steady shear, time dependent shear behavior, and oscillatory linear viscoelasticity (LVE) of the suspensions are reported and remarkably strong similarities were observed between the CB and CNT suspension rheology, for example, 4 wt. % CB and 0.4 wt. % CNT suspensions. Optical observations showed that both the CB and CNT microstructures were shear rate sensitive and a structure-dependent hybrid Maxwell-Voigt phenomenological model with a yield stress was developed that gave a reasonable fit to the rheological data. The structure model parameters for both systems were found to be of a similar order of magnitude, although the onset of rheology development for the two systems occurred with a decade difference of concentration. The experimental rheological results and model fit indicated that for both CB and CNT suspensions, the observed rheology changes were dominantly controlled by aggregate size and interaction, rather than the respective particulate and filament morphology of the CB and CNT microstructures. The critical concentration for the onset of rheology development was, however, dependant on the basic morphology of the CB and CNT suspensions. © *2012 The Society of Rheology*. [http://dx.doi.org/10.1122/1.4751871]

I. INTRODUCTION

Carbon black (CB) and carbon nanotubes (CNTs) are both nanoscale forms of graphitic carbon, although their internal structures and morphology differ. CB base particles are essentially spherical, with diameters between 30 and 50 nm; however, the particles usually exist in a fused assembly to form larger structures with average diameters between 0.1 and 0.8 μm [see for example, Barrie *et al*. (2004); Bigg (1984)]. These larger structures may take on many different morphological forms such as spherical, ellipsoidal, and complex fractal shapes [see for example Aoki *et al*. (2003); Barrie *et al*. (2004)].

[a]Author to whom correspondence should be addressed; electronic mail: katyearsley@gmail.com

© 2012 by The Society of Rheology, Inc.

Downloaded 29 Nov 2012 to 81.132.17.87. Redistribution subject to SOR license or copyright; see http://www.journalofrheology.org/masthead

CNTs consist of graphene sheets rolled into tubes. The diameters of the tubes are of the order of 1–100 nm and the lengths are usually up to the μm range, meaning that the aspect ratios of the CNTs are significantly larger than the CB structures [Iijima (1991); Singh *et al.* (2003)]. In terms of CNTs, this paper is concerned with multiwalled carbon nanotubes (MWNTs) which consist of multiple concentric graphene cylinders and MWNTs are currently the most commercially available form of CNT.

CB has been used for many decades as a polymer additive for protection from ultraviolet light, increased toughness, improved processability, and enhanced electrical conductivity [see for example Grayson *et al.* (1978); White and Crowder (1974)]. However, the relatively high CB loading required for conductivity applications in particular can result in a brittle final composite [Bigg (1984); Sandler *et al.* (1999)]. More recently, CNTs have been proposed as better candidates for both thermoplastic and thermoset polymer fillers compared to CB because of the superior intrinsic properties of the CNTs such as very high mechanical stiffness and strength, combined with low density and high thermal and electrical conductivities [Fischer *et al.* (1997); Jin *et al.* (1998); Kim *et al.* (2001); Krishnan *et al.* (1998)]. The high aspect ratio of the CNTs compared to CB means that they should potentially be able to mechanically reinforce the polymer matrix and also that the electrical percolation threshold is much lower for CNTs compared to CB [Alig *et al.* (2011)].

The rheological behavior of CB suspensions has been investigated extensively over many years since the 1970s [see, for example, Lobe and White (1979); Mewis and Schoukens (1978); White and Crowder (1974)]. Similarly, since their discovery in the 1990s [Iijima (1991)], CNTs in suspension have also been studied [see for example reviews by Ma *et al.* (2008b); Nobile (2011)]. Nevertheless, as yet there does not appear to have been a systematic comparison of CB with CNTs as presented in this paper. Such an assessment is beneficial as it allows the shape effects of the essentially isotropic CB and anisotropic CNTs to be determined where CB and CNTs are both nanoscale structures of the same graphitic carbon. Furthermore, the relatively new CNTs suspension materials can be ranked against the well established technology of CB currently being used as a polymer filler.

This paper reports rheological data for CB and MWNTs suspended in the same Newtonian epoxy resin and subjected to the same flow conditions, thereby enabling a direct comparison of performance. Optical microscopy of both CB and MWNT suspensions during and immediately after shear was also carried out which allowed the structures formed by the filler particles to be observed. Hence the links between the microstructure of the dispersions and their rheological behaviour could be better understood. In addition, a structure-dependent mechanical analogue model was developed and fitted to all the rheological data in order to explore the quantitative behavior of the two systems and help provide some insight into the deformation mechanisms of the two systems.

II. MATERIALS AND EXPERIMENTAL PROTOCOL

A. CB and MWNT dispersions

MWNTs were supplied by the Macromolecular Materials Laboratory at the Department of Materials Science and Metallurgy, University of Cambridge. The MWNTs were formed by chemical vapor deposition from toluene in the presence of an iron catalyst as described by Singh *et al.* (2003). Characterization of the MWNTs by scanning electron microscopy carried out by Singh *et al.* revealed that the CNTs grew in aligned mats of high purity nanotubes and that the MWNTs had diameters of typically less than 100 nm.

Downloaded 29 Nov 2012 to 81.132.17.87. Redistribution subject to SOR license or copyright; see http://www.journalofrheology.org/masthead

Assessment of the CNT length is difficult and SEM and optical microscope observations suggested length scales of order 100 μm before dispersion.

Cabot Vulcan XC72R CB was obtained from the Cabot Corporation (www.cabot-corp.com). This is a commercially manufactured CB which has been specifically developed for electrostatic discharge applications, meaning it has a high electrical conductivity but is also known to improve the stiffness of composite materials [Cabot Corporation (2008)]. Characterization of Cabot Vulcan XC72R by Tomantschger and Kordesh (1989) and Hu *et al.* (2011) has revealed a fractal structure with particle diameters of around 30 nm.

An epoxy resin (UV 60-7155; Epoxies Etc—www.epoxies.com) was used as the suspending medium. The epoxy contained a photoinitiator which would cause it to cure in the presence of ultraviolet light; however, UV was not used in the rheological experiments described in this paper.

CB or CNTs were dispersed in the epoxy using a high-powered ultrasound apparatus (Sonicbio NR-300; www.diagenode.com). Suspensions were made at the concentrations required for experiments meaning there was no further dilution required beyond the initial dispersion process. Each batch of 15 g samples received a total of four 15 min treatment sessions in the ultrasound apparatus which consisted of a repeated cycle of 30 s of ultrasound followed by 30 s of rest. After the initial dispersion process, samples of the same concentration were mixed together and transferred to glass jars which were kept out of direct sunlight. Before use, the suspensions were stirred manually to redisperse any settled CB or CNTs.

Relatively large attractive London-van der Waals forces exist between the long, thin structures of the CNTs [Ahir *et al.* (2008)]. Therefore, the formation of stable homogeneous suspensions of CNTs remains a complex issue, although the use of surfactants [see for example Lisunova *et al.* (2006)] and CNT functionalization by chemical pretreatment methods [see for example Kinloch *et al.* (2002); Park *et al.* (2003)] has been shown to improve dispersion quality. Nevertheless, functional groups added to the surfaces of CNTs can distort the planar sp^2 geometry of the carbon atoms and reduce the electrical conductivity of the nanotubes [Bose *et al.* (2010); Park *et al.* (2009)] and hence the suspensions used in this paper were made without any chemical pretreatment.

B. Optical microscopy

Optical microscopy studies were carried out using a Cambridge Shear System (CSS) manufactured by Linkam Scientific Instruments [Bower *et al.* (1998); Mackley *et al.* (1999)]. The shear cell consists of two parallel quartz plates, the top of which is fixed, whereas the bottom can rotate using a stepper motor. The gap size was set at 50 μm. The samples were viewed using an optical microscope combined with a JVC color video camera (TK-C1480E) at a distance of 7.5 mm from the center of the plates. Optical experiments were performed at ambient temperature (20–25 °C).

C. Rheological experiments

Rheological experiments were carried out using an advanced rheometric expansion system (ARES) controlled-strain rheometer (TA Instruments). 50 mm parallel plates were used with a gap size of 0.5 mm. To allow for the nonconstant shear rate across the plates, corrections of the type suggested by Carvalho *et al.* (1994) were applied to the steady shear data but it was felt that the difference between the corrected and uncorrected values was insignificant and therefore only raw data are presented in this paper. The temperature for all rheological experiments was maintained using a forced air oven at 25 °C. Steady shear,

Downloaded 29 Nov 2012 to 81.132.17.87. Redistribution subject to SOR license or copyright; see http://www.journalofrheology.org/masthead

step rate, and oscillatory LVE experiments were performed. Normal stress data were not measured owing to the difficulty of obtaining reliable data with this sort of system.

III. EXPERIMENTAL RESULTS

A. Optical microscopy

Representative optical micrographs of low concentration CB and MWNT suspensions are given in Fig. 1 and clearly demonstrate differences between the CB and MWNT structures. As shown in Fig. 1(a), the CB appeared as essentially isotropic, approximately spherical structures, whereas the resolvable MWNT structures, although unlikely to be individual nanotubes at this magnification, had high aspect ratio fibre structures. The CNT structures are of the order of 10–50 μm long, which is shorter than the undispersed MWNTs and so it is likely that the sonication dispersion process has resulted in CNT breakage. As shown in Fig. 2, in the absence of shear, as the filler particle concentration was increased, the CB particles formed increasingly larger and denser aggregates resulting in a coarsening optical texture as shown in Figs. 2(a)–2(c). In terms of quiescent optical structures of MWNTs shown in Figs. 2(d)–2(f), at 0.2 wt. %, the CNT structures form an approximately uniform network across the suspension [Fig. 2(e)] although large CNT aggregates were also formed within the network at 0.5 wt. % MWNTs [Fig. 2(f)].

It was found that the observed optical microstructures of the CB and CNT suspensions were sensitive to the applied shear rate and this effect is shown for both CB and CNT in Fig. 3. Samples of both CB and MWNTs sheared at 0.5 s^{-1} for several minutes contained large aggregates and increasing the shear rate to 10 and 100 s^{-1} resulted in progressively smaller aggregates, demonstrating the importance of high shear rates for good dispersion of both CB and MWNTs. Shearing the sample once more at 0.5 s^{-1} resulted in the reformation of the large aggregates showing the reversible nature of the aggregation process. The optical micrograph of the high shear MWNT suspension, Fig. 3(f), also indicates that some CNT orientation in the direction of flow has occurred. The effect of shear on aggregate size has been reported independently for CB [Osuji and Weitz (2008)] and CNTs [see for example Lin-Gibson *et al.* (2004); Hobbie and Fry (2007); Ma *et al.* (2008a); Rahatekar *et al.* (2006)] as well as other nanocomposite systems [see for example Mobuchon *et al.* (2009)] and the results here confirm the similarities of those findings for the systems investigated in this paper.

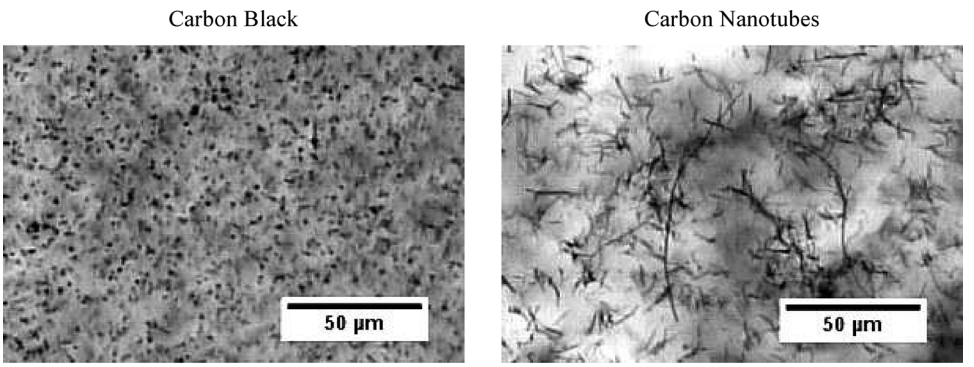

FIG. 1. CB and MWNT suspensions following dispersion: Optical micrographs, taken using the CSS with 50 μm gap, of (a) 0.1 wt. % CB and (b) 0.25 wt. % CNTs in liquid epoxy. The CB structures appear isotropic, whereas the CNT structures have much larger aspect ratios.

Downloaded 29 Nov 2012 to 81.132.17.87. Redistribution subject to SOR license or copyright; see http://www.journalofrheology.org/masthead

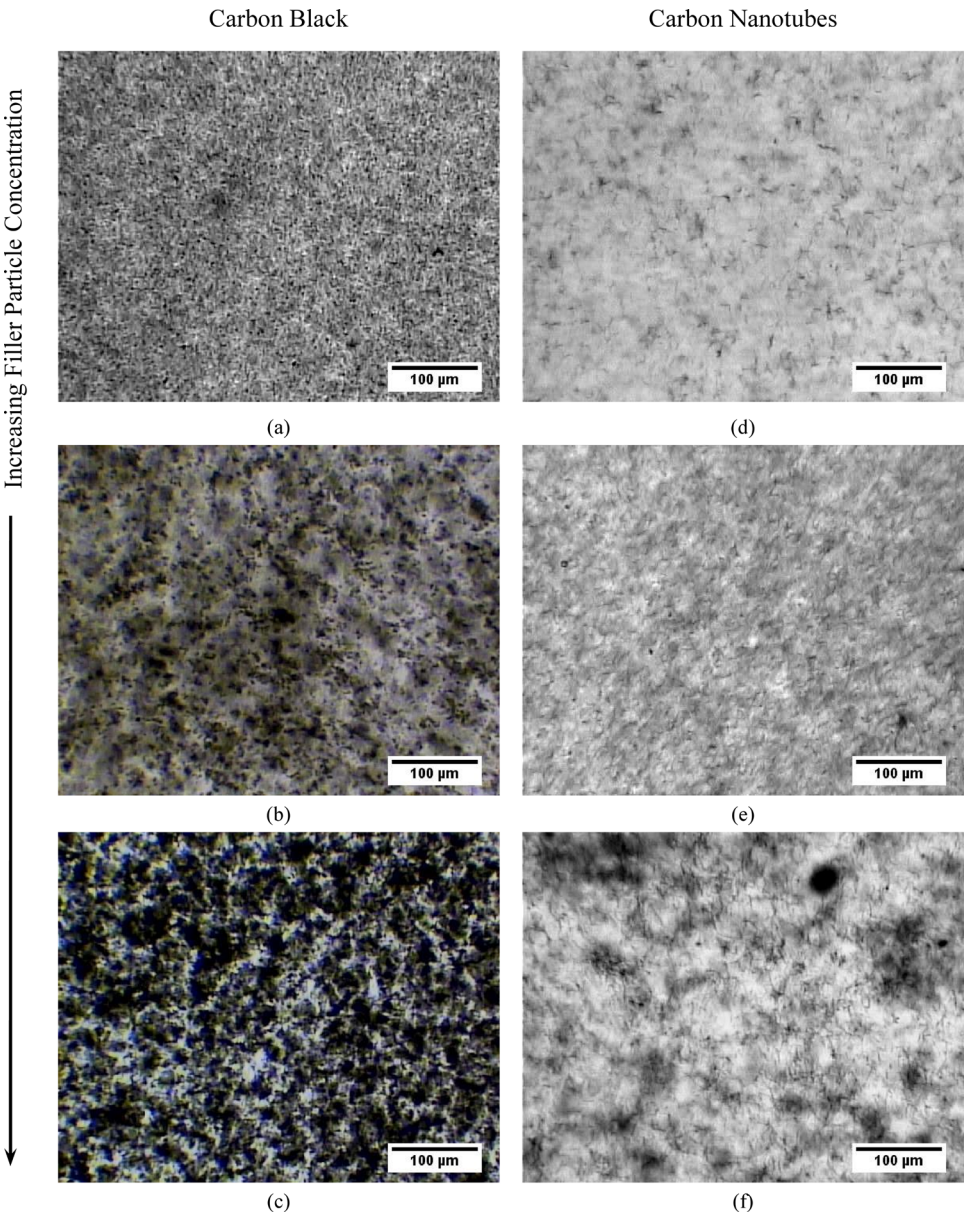

FIG. 2. Increasing the concentration of CB or CNTs (shown by the direction of the arrow) results in a coarser microstructure: (a) 0.1 wt. % CB; (b) 0.25 wt. % CB; (c) 0.5 wt. % CB; (d) 0.03 wt. % CNT; (e) 0.2 wt. % CNT; (f) 0.5 wt. % CNT. Taken using the CSS with 50 μm gap.

It should be noted that the relatively long lengths of the MWNT structures ($\sim$10–50 μm) compared to the small gap size required for optical imagery (50 μm) means that there is the potential for the microstructures formed to be influenced by the confinement of the CNTs [Lin-Gibson *et al.* (2004)]. The smaller size of the CB structures means that confinement is less likely to be an issue for the CB suspensions. Nevertheless, even when the MWNT dispersions were subjected to low shear for long periods of time (4 h), the banded structures observed by both Lin-Gibson *et al.* (2004) and Ma *et al.* (2008a), and associated with confined aggregate growth, were not seen in this system.

Downloaded 29 Nov 2012 to 81.132.17.87. Redistribution subject to SOR license or copyright; see http://www.journalofrheology.org/masthead

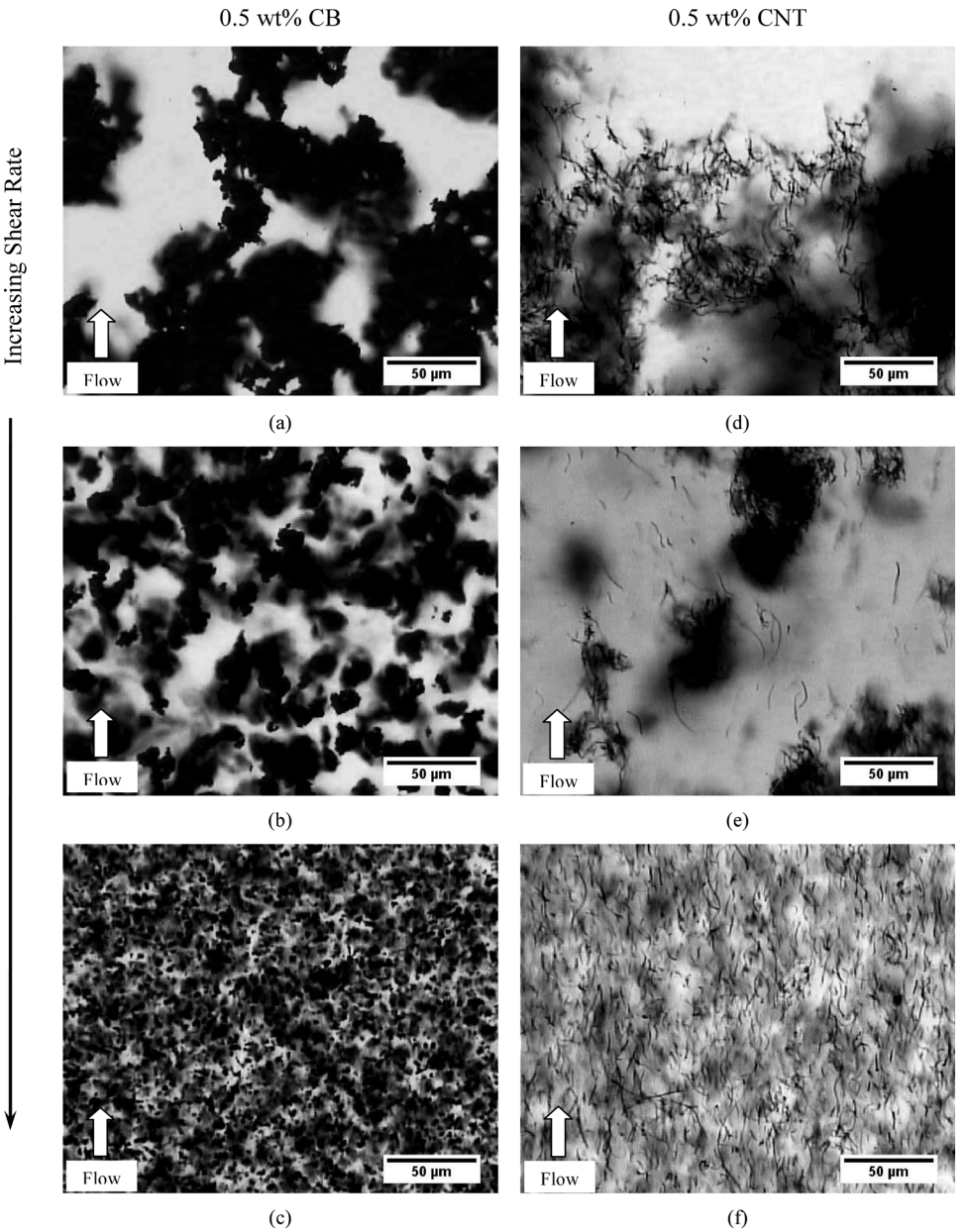

FIG. 3. Increasing the shear rate in the direction of the arrow results in smaller CB or CNT aggregates: 0.5 wt. % CB after (a) 15 min at $0.5\,s^{-1}$; (b) 1 min at $10\,s^{-1}$ (c) 1 min at $100\,s^{-1}$; 0.5 wt. % CNT after (d) 15 min at $0.5\,s^{-1}$; (e) 1 min at $10\,s^{-1}$; (f) 1 min at $100\,s^{-1}$. Taken immediately after shear using the CSS with 50 μm gap.

B. Steady shear rheology

The variation of steady shear apparent viscosity, η, with shear rate is shown in Fig. 4 for multiple concentrations of CB and MWNT in epoxy. The epoxy resin without any filler is Newtonian with a constant viscosity of 0.47 Pa s. The steady shear behavior of the 0–6.0 wt. % CB and 0–0.6 wt. % MWNT suspensions appears remarkably similar with both showing shear thinning characteristics that asymptote toward a high shear rate

Downloaded 29 Nov 2012 to 81.132.17.87. Redistribution subject to SOR license or copyright; see http://www.journalofrheology.org/masthead

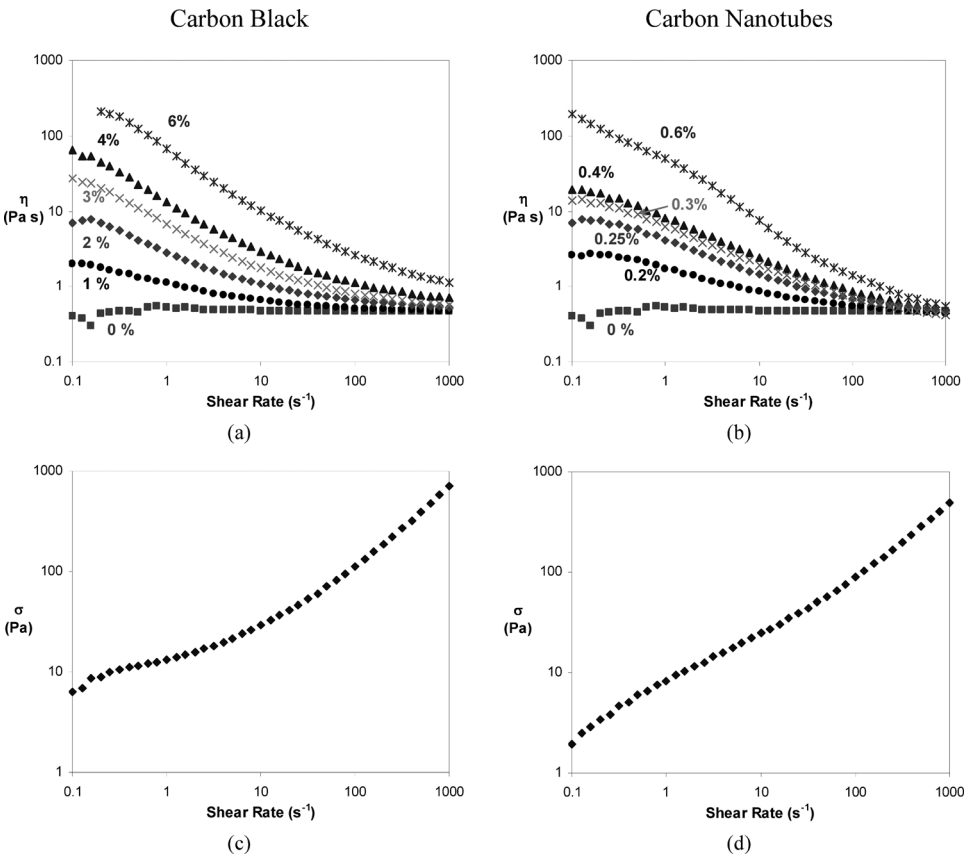

FIG. 4. CB and MWNT suspensions show shear thinning behavior: Steady shear apparent viscosity at 25 °C as a function of shear rate for (a) CB and (b) CNT suspensions in epoxy. The suspensions also seem to tend toward a yield stress at low shear: (c) 4% CB and (d) 0.4% MWNT.

viscosity approaching that of the matrix alone. Similar shear thinning behavior of both CB and CNT dispersions has been independently documented before but not directly compared [see for example Kawaguchi *et al.* (2001); Ma *et al.* (2008a); Nobile (2011); Schoukens and Mewis (1978)].

For both CB and MWNT suspensions, the low shear rate apparent viscosity of the suspensions in Fig. 4 increases with increasing filler particle concentration; however, to obtain comparable magnitudes of viscosity enhancement, it was necessary to use a significantly larger loadings of CB than CNTs. For example, a 6 wt. % CB suspension in Fig. 4(a) has a similar apparent viscosity at $1\,s^{-1}$ as a 0.6 wt. % CNT suspension in Fig. 4(b). Plots of shear stress against shear rate appear to show a yield stress of between 1 and 10 Pa for the 4 wt. % CB and 0.4 wt. % MWNT suspensions [Figs. 4(c) and 4(d)].

C. Step rate experiments

Within an aggregating suspension such as the CB or MWNT dispersions in epoxy, Mewis and Wagner (2010) identify three possible contributions to the total stress of the system, namely the hydrodynamic, viscoelastic, and thixotropic stresses. The relative contributions of each can be appreciated by considering the response of the suspension to

Downloaded 29 Nov 2012 to 81.132.17.87. Redistribution subject to SOR license or copyright; see http://www.journalofrheology.org/masthead

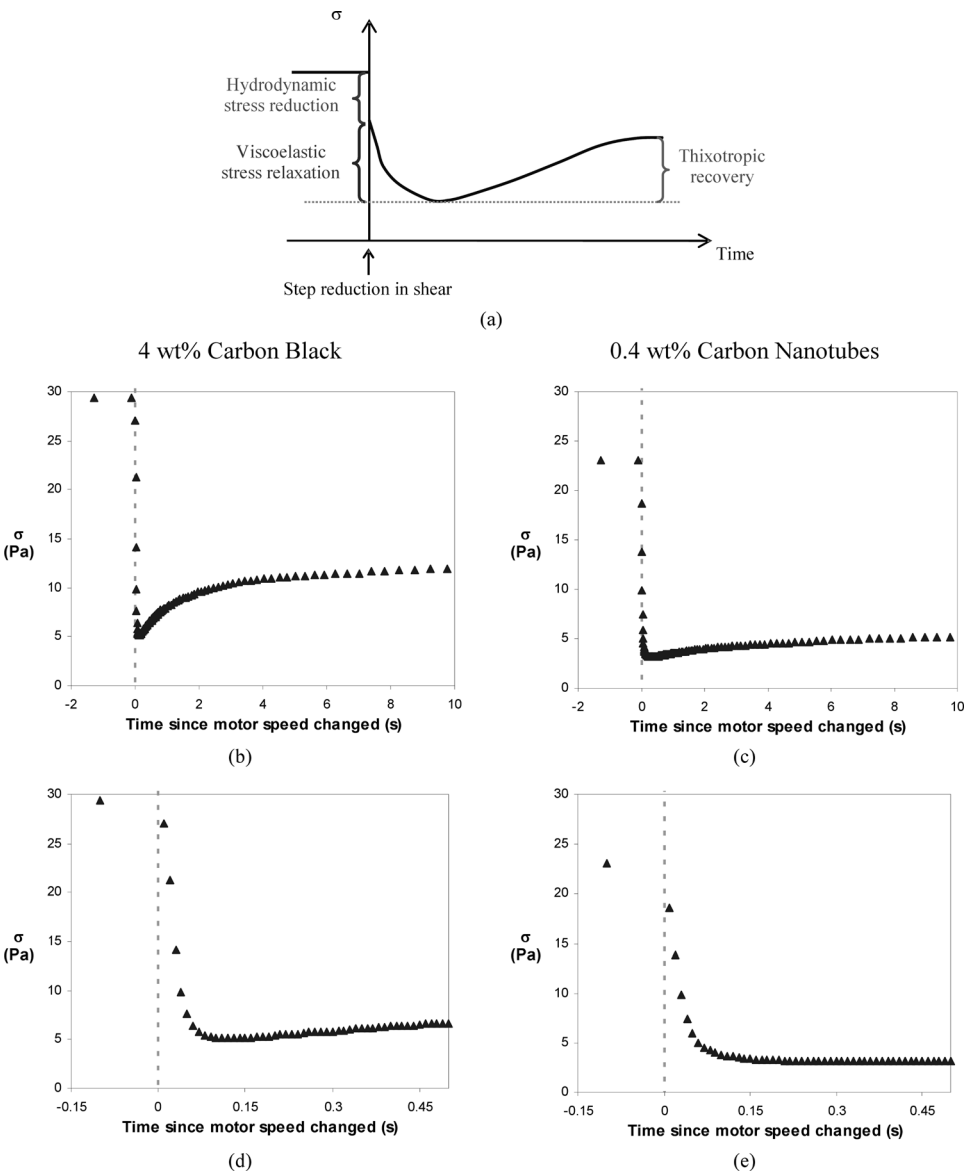

FIG. 5. Response of a reversibly flocculating suspension to a step reduction in shear rate: (a) Schematic of the general thixotropic response as discussed by Mewis and Wagner (2010); (b) 4 wt. % CB and (c) 0.4 wt. % MWNT in epoxy following a step reduction in shear from $10\,s^{-1}$ to $0.5\,s^{-1}$; (d) 4 wt. % CB and (e) 0.4 wt. % MWNT on a larger scale showing the viscoelastic relaxation process in detail.

a step reduction in rate, as shown schematically in Fig. 5(a). The hydrodynamic stress arises from the viscous drag between the solvent and the filler and is strongly influenced by the shear rate of the fluid. Hence, in Fig. 5(a), the hydrodynamic stress responds immediately to the change in shear rate, whereas the viscoelasticity of the suspensions results in stress relaxation over slightly longer times. The thixotropic stress, which arises from the change in microstructure of the dispersion, has the longest characteristic timescale of the three stresses and increases with time as the average aggregate size increases at the lower shear rate.

Downloaded 29 Nov 2012 to 81.132.17.87. Redistribution subject to SOR license or copyright; see http://www.journalofrheology.org/masthead

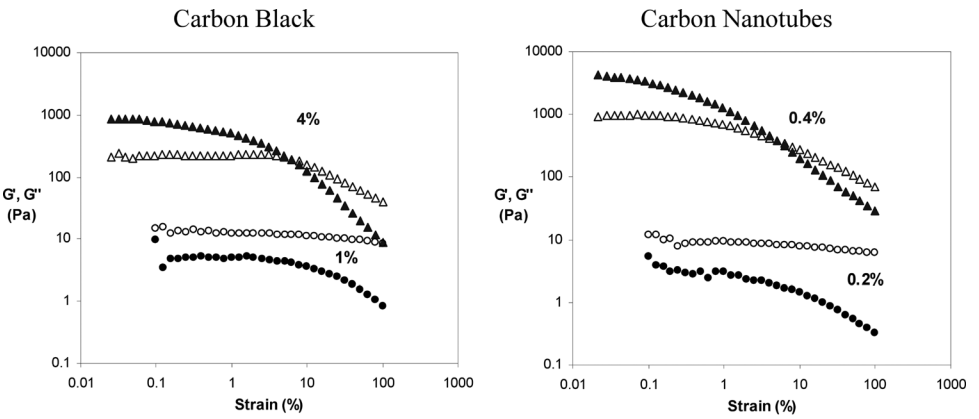

FIG. 6. More concentrated CB or CNT suspensions show nonlinear behavior at lower strains: Strain sweep data recorded at 10 rad s^{-1}, 25 °C for (a) CB and (b) MWNT suspensions.

The response of the 4 wt. % CB and 0.4 wt. % MWNT suspensions to a step reduction in shear from 10 to 0.5 s^{-1} is shown in Figs. 5(b) and 5(c). Both suspensions show ~10% reduction in stress due to hydrodynamic effects and a short timescale (~0.1 s for 4 wt. % CB and ~0.2 s for 0.4 wt. % MWNT) viscoelastic relaxation preceding a much longer thixotropic recovery period. The viscoelastic relaxation can be seen more clearly in the large scale plots in Figs. 5(d) and 5(e). Again the rheological responses of the CB and MWNT suspensions are remarkably similar although the suspension loadings required to observe similar effects are significantly different.

D. Oscillatory LVE

The linear viscoelastic regions of the CB and MWNT suspensions were established by performing strain sweep experiments at a fixed oscillation frequency of 10 rad s^{-1}. As the concentration of the suspensions increased, the storage modulus G' and loss modulus G'' exhibited nonlinear behavior at lower strains, as shown in Fig. 6. To strike a balance between generating sufficient torque for accurate readings whilst remaining within the LVE region of the suspension, lower strains were used for more concentrated dispersions during the LVE frequency sweep experiments, as shown in Table I.

The frequency dependence of G' and G'' for suspensions not subject to any preshear is shown in Fig. 7. As with the steady shear viscosity, the LVE behavior of the CB and MWNT suspensions appear remarkably similar although the concentrations of the CB suspensions (1–6 wt. %) are about ten times larger than for the MWNT suspensions (0.2–0.6 wt. %). Both G' and G'' increase upon the addition of CB or CNTs, although the

TABLE I. Strain amplitudes used during frequency sweep oscillatory LVE experiments.

Strain	Suspension
50%	Epoxy
1%	1% CB; 2% CB; 3% CB
	0.2% MWNT; 0.25% MWNT; 0.3% MWNT
0.1%	4% CB; 6% CB
	0.4% MWNT; 0.6% MWNT

Downloaded 29 Nov 2012 to 81.132.17.87. Redistribution subject to SOR license or copyright; see http://www.journalofrheology.org/masthead

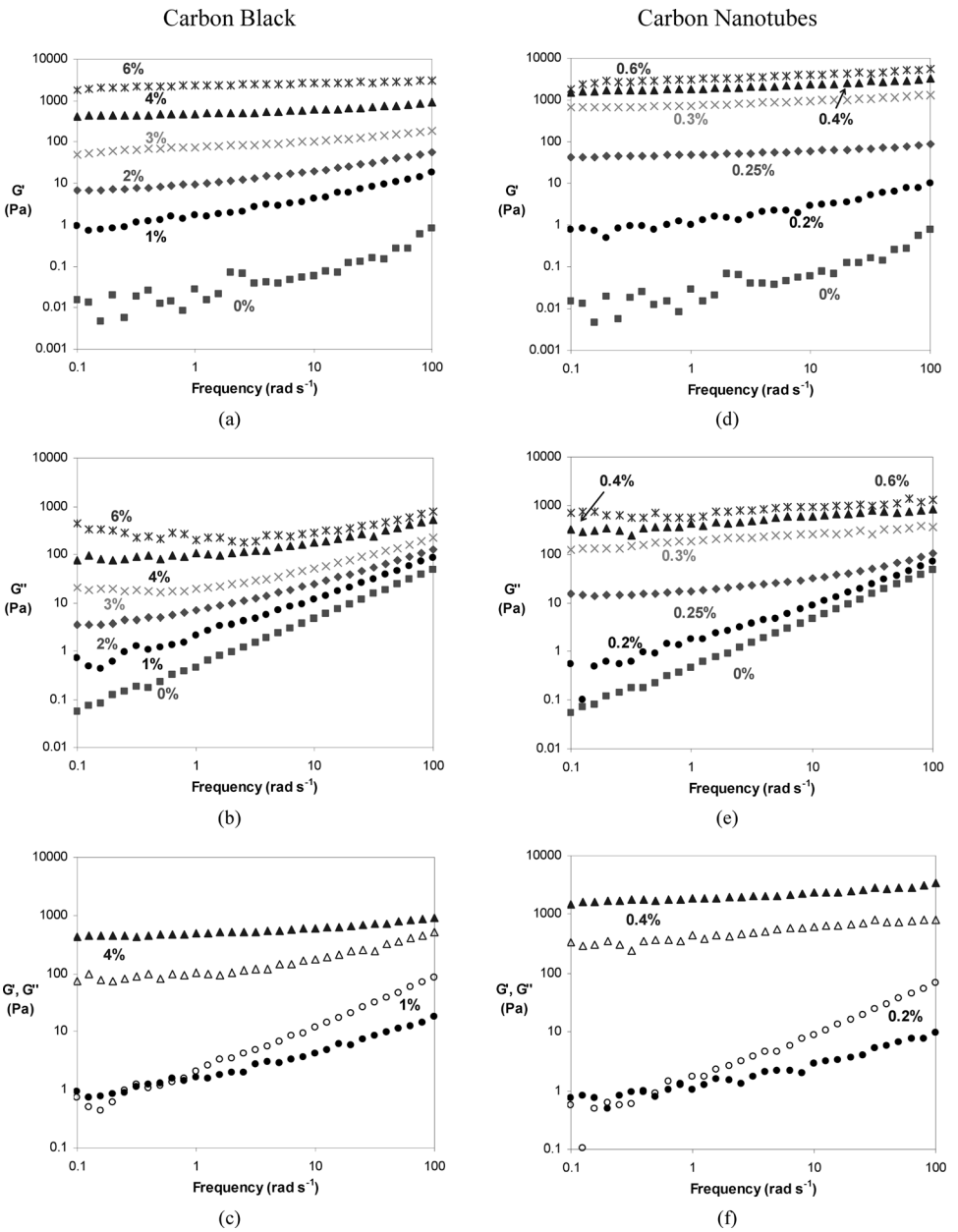

FIG. 7. LVE behavior of CB and CNT suspensions: (a) G' and (b) G'' for CB dispersions; (c) G' (closed symbols) and G'' (open symbols) for 1 wt. % and 4 wt. % CB; (d) G' and (e) G'' for CNT dispersions; (f) G' (closed symbols) and G'' (open symbols) for 0.2 wt. % and 0.4 wt. % MWNT.

increase in G' is more significant such that G' is dominant across all frequencies tested for the higher concentration dispersions [Figs. 7(c) and 7(f)]. With increased loading, G' shows less dependence on frequency and a low frequency plateau exists for suspensions ≥ 3 wt. % CB and ≥ 0.25 wt. % MWNT. This behavior has been observed for CB and CNT suspensions independently elsewhere [see for example Aoki *et al.* (2003); Ma *et al.* (2008a)] and the observations are consistent with the formation of a percolated filler particle network.

Downloaded 29 Nov 2012 to 81.132.17.87. Redistribution subject to SOR license or copyright; see http://www.journalofrheology.org/masthead

Although there are similarities between the rheological and electrical percolation thresholds for composite systems as both require the formation of some sort of filler particle network, the actual percolation mechanism is slightly different in each case. For rheological percolation, the filler particles must restrain the long range relaxation process of the matrix, whereas for electrical percolations, the conductivity CB or CNT structures must be close enough together for electron transfer [see for example Du *et al*. (2004); Hu *et al*. (2006); Nobile (2011)]. Electrical conductivity measurements presented elsewhere [Yearsley (2011)] demonstrated electrical percolation at 3 wt. % CB and 0.2 wt. % CNTs. The lower CNT concentration required for electrical percolation than rheological percolation was attributed to the presence of electron tunneling which allowed charge transfer between CNTs without them fully touching. The absence of long chains in the epoxy matrix, however, meant that a physical network of touching CNTs was required for rheological percolation. A similar argument was presented by Chapartegui *et al*. (2010).

The CB or CNT microstructure in a suspension can be altered by preshearing the dispersions before the frequency sweep experiments. Figure 8 shows G′ and G″ for 4 wt. % CB and 0.4 wt. % MWNT suspensions without preshear and after preshear at $1\,s^{-1}$ for 10 min, $10\,s^{-1}$ for 1 min, and $100\,s^{-1}$ for 1 min. In general, it takes longer for a stable microstructure to be formed at lower shear, but optical microscopy and transient steady shear viscosity measurements [presented in detail by Yearsley (2011)] indicated that the

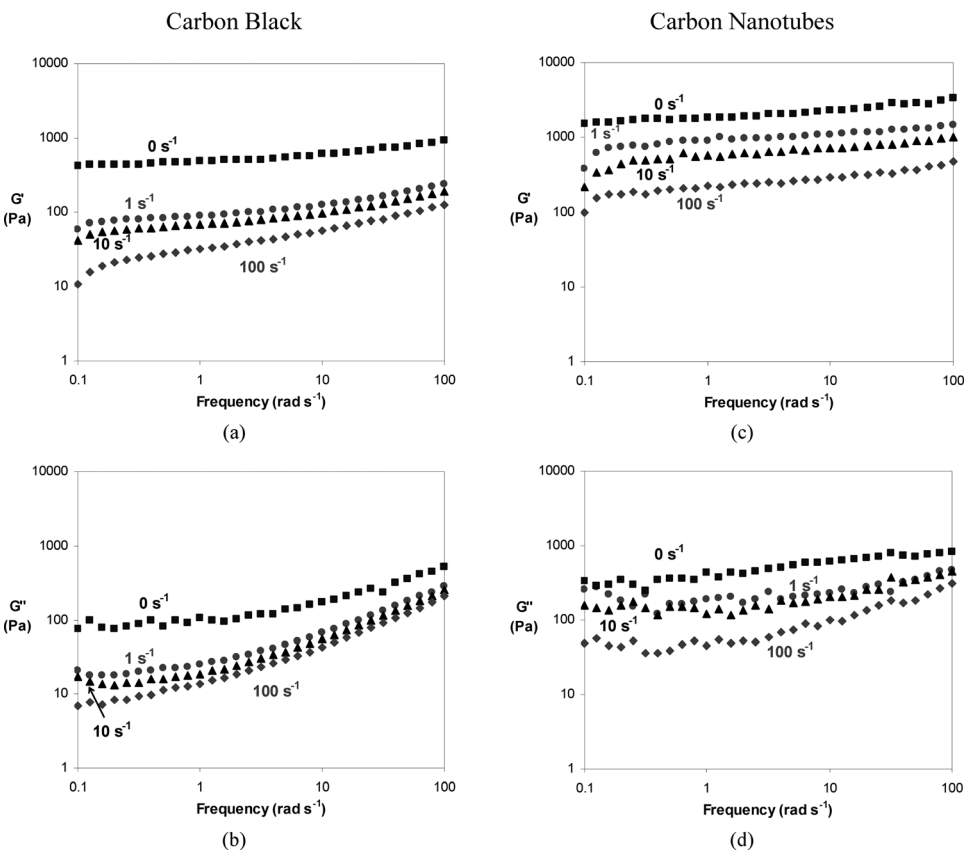

FIG. 8. G' and G'' after 60 min of rest following sample loading (marked $0\,s^{-1}$), and after preshear at $1\,s^{-1}$ for 10 min, $10\,s^{-1}$ for 1 min, and $100\,s^{-1}$ for 1 min: 4 wt. % CB (a) G', (b) G''; 0.4 wt. % MWNT (c) G', (d) G''.

Downloaded 29 Nov 2012 to 81.132.17.87. Redistribution subject to SOR license or copyright; see http://www.journalofrheology.org/masthead

suspensions would be at quasi steady state under these conditions. In the absence of preshear, both suspensions show low frequency plateaus in G', consistent with the presence of a percolated filler particle network. G' and G'' are lower for the samples which were subjected to preshear and G' and G'' decrease with increasing preshear rate.

Both the CB and CNT suspensions exhibited an increase or "recovery" in G' with time following preshear, as shown in Fig. 9 for the 4 wt. % CB and 0.4 wt. % MWNT dispersions at 10 rad s^{-1}. For both suspensions, the dG'/dt gradient decreases significantly over the first 50 s and tends toward zero after ~200 s. It is possible, therefore that the low frequency readings of G' in Fig. 8 do not reflect dispersions at steady state and should be treated with caution. However, since the rheometer took ~100 s for each LVE measurement below 0.2 s^{-1}, it is thought that the remainder of the data in Fig. 8 was taken at steady state.

G' recovery following preshear has been reported elsewhere for CNT suspensions [see for example Alig *et al.* (2008); Skipa *et al.* (2010)] and has been attributed to both microstructure evolution on a submicron scale [Khalkhal *et al.* (2011)] and the elastic recovery of nanotubes entangled within aggregates which were stretched during flow [Pujari *et al.* (2011)]. It is possible that both effects are occurring within the CNT system, although the CB suspensions can only show recovery by microstructure evolution as the structure of the CB particles means that they are unlikely to deform elastically under flow in the same way as the CNTs. It is interesting, therefore, that the magnitude of the G' recovery as a percentage of the initial value is comparable for the CB and CNT suspensions plotted in Fig. 9 if the recovery mechanisms of the two dispersions differ.

IV. RHEOLOGICAL MODELING OF CB AND CNT SUSPENSIONS

It has been shown that the rheological characteristics of the CB and MWNT suspensions are strongly influenced by the shear history of the dispersions. In particular, low shear has been seen to promote the formation of large aggregates which are broken down under high shear. Whilst the anisotropic nature of the MWNT structures has resulted in differences between the behavior of the CB and CNT suspensions in terms of a percolation threshold concentration, filler particle aggregation and disaggregation with shear is

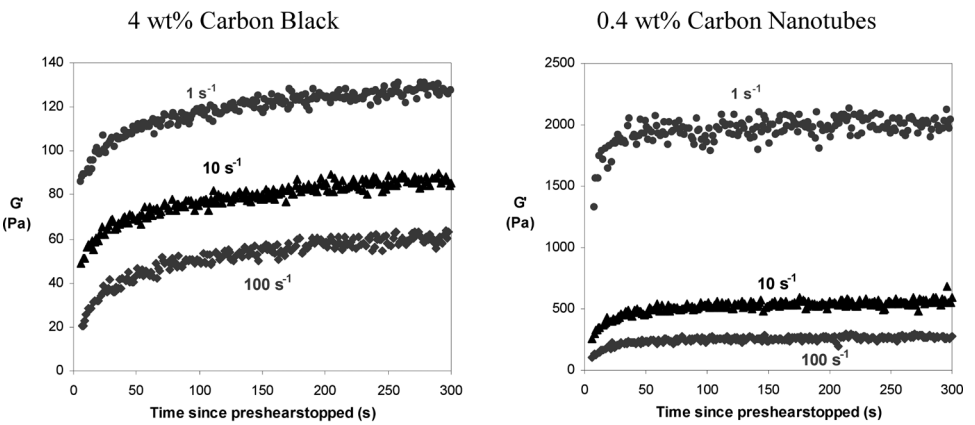

FIG. 9. G' recovery with time following preshear at 1 s^{-1} for 5 min, 10 s^{-1} for 1 min or 100 s^{-1} for 1 min: (a) 4 wt. % CB (b) 0.4 wt. % MWNT. Readings were taken at 10 rad s^{-1}, 25 °C.

Downloaded 29 Nov 2012 to 81.132.17.87. Redistribution subject to SOR license or copyright; see http://www.journalofrheology.org/masthead

thought to be the dominant process for both dispersions. Therefore, a model was developed which linked the rheological characteristics of the dispersions to the state of aggregation, represented by a structure parameter, ε, which denotes the number fraction of aggregated filler particles. A mechanical analogue was devised for the CB and CNT suspensions and the parameters in the model were related to ε. The rate of change of ε was made dependent on the shear rate experienced by the dispersions. Similar structural kinetics models have been devised for CB dispersions [see for example Dullaert and Mewis (2006); Mewis and Wagner (2009); Quemada (1998)] and other thixotropic systems [see for example Yziquel *et al*. (1999)] but have not been extensively applied to CNT suspensions.

A. Mechanical analogue model

A mechanical analogue model, shown schematically in Fig. 10(a), was developed for the CB and CNT suspensions which initially separates the viscous effects of the solvent and the hydrodynamic and viscous effects of the filler in a manner similar to Coussot and Leonov (1993) and Mujumbar *et al*. (2002). The solvent and hydrodynamic contributions to the total stress, being viscous in origin, are represented as dashpots with viscosities η_s and η_h, respectively. The viscoelasticity arising from the filler is represented by a Maxwell element with spring constant g and relaxation time λ. Data from step rate experiments shown in Fig. 5 have shown that the viscoelastic effects of the filler are only active over relatively short timescales during shear, corresponding to small sample deformations. Dullaert and Mewis (2006) have therefore argued that the elastic strain should have a limiting or critical value. This concept was incorporated into the mechanical analogue shown in Fig. 10(a) through the use of a "slider" yield stress which limits the stress that can be supported by the Maxwell element to σ_c, as shown in Fig. 10(b). Within the LVE

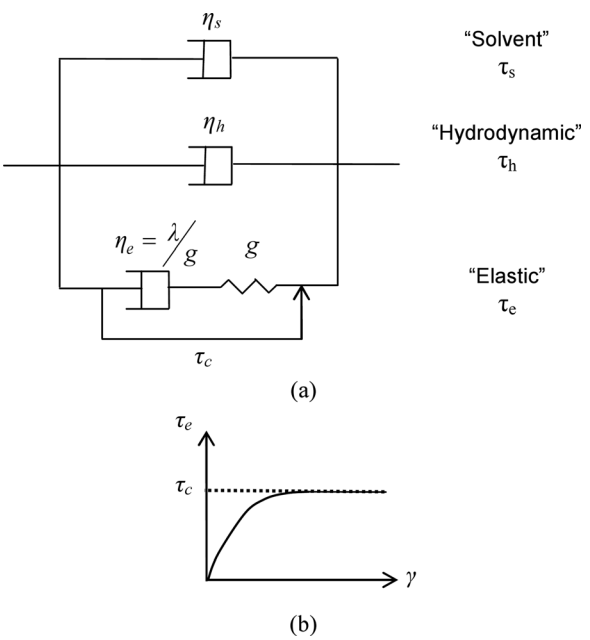

FIG. 10. (a) The mechanical analogue for the CB and CNT suspensions, termed the "structure-dependent hybrid Maxwell-Voigt phenomenological model with yield stress"; (b) the effect of the slider is to limit the maximum stress an element can support at large strains.

Downloaded 29 Nov 2012 to 81.132.17.87. Redistribution subject to SOR license or copyright; see http://www.journalofrheology.org/masthead

region, the slider is not active and the "elastic" part of the model behaves according to a standard Maxwell element. At large deformations outside the LVE regime, the stress across the Maxwell element is limited to σ_c, allowing nonlinear behavior to be modeled.

As the filler particles move past each other in suspensions under shear, they will continuously be breaking and reforming interactions with their neighboring aggregates. For steady deformation, with time a dynamic equilibrium is reached for the total number of interactions within the dispersion and this relates to the critical stress σ_c. The solvent viscosity, η_s, is unaffected by the filler particles but the other model parameters vary with ε, as proposed by Quemada (1999). For simplicity, and to minimize the number of fitting parameters, it is assumed that η_h, σ_c, g, and λ have a linear dependence on ε as

$$\eta_h = A\varepsilon, \tag{1}$$

$$\sigma_c = B\varepsilon, \tag{2}$$

$$g = C\varepsilon, \tag{3}$$

$$\lambda = D\varepsilon, \tag{4}$$

where A, B, C, and D are fitting parameters. Given that the CB and MWNT suspensions have been shown to exhibit percolation behavior, it is likely that the linear dependence is an oversimplification, but it is acceptable over the concentration range investigated here. As ε tends to zero, Eqs. (1)–(4) indicate that the shear stress in the suspension tends to the solvent contribution only; however, a detailed analysis of such behavior is not presented here.

As the model incorporates concepts from both the Voigt (viscous and elastic elements in parallel) and Maxwell (viscoelasticity arises from a spring and dashpot in series) models for viscoelasticity, the model was termed the "structure-dependent hybrid Maxwell-Voigt phenomenological model with yield stress." The model has been developed for data obtained using a controlled strain rheometer and is not necessarily as easily applied to a controlled stress environment.

B. Kinetic equation for the structure parameter

Shear can act to both increase the number of aggregated particles, by bringing unaggregated structures together or decrease ε by pulling aggregates apart. The constructive effects of shear are represented by V_c and are assumed to act on the unaggregated filler particles. Similarly, the destructive effects of shear are represented by V_d and are assumed to act on the aggregated filler particles. It is therefore possible to write a kinetic equation for ε as

$$\frac{d\varepsilon}{dt} = V_c(1-\varepsilon) - V_d\varepsilon. \tag{5}$$

V_c contains both a shear rate dependent term and a shear rate independent term which accounts for microstructure recovery in the absence of shear as

$$V_c = k_1\dot{\gamma}^a + k_2. \tag{6}$$

V_d contains only a shear rate dependent term as

$$V_d = k_3\dot{\gamma}^b. \tag{7}$$

Downloaded 29 Nov 2012 to 81.132.17.87. Redistribution subject to SOR license or copyright; see http://www.journalofrheology.org/masthead

k_1, k_2, k_3, a, and b are fitting parameters. Similar expressions to Eqs. (5)–(7) have been used by others to describe the behavior of reversibly flocculating suspensions, as detailed in the review by Mewis and Wagner (2009).

C. Model forms for different rheological experiments

The nature of the rheological deformation affects the form of the model which should be used.

1. Steady shear

Under steady shear, the suspensions are subject to large deformations and therefore the slider in the model is active. At steady state, $d\varepsilon/dt = 0$ and hence the steady state value of ε at a given shear rate, denoted by ε_{ss}, can be obtained from

$$\varepsilon_{ss} = \frac{V_c}{V_c + V_d} = \frac{k_1\dot{\gamma}^a + k_2}{k_1\dot{\gamma}^a + k_2 + k_3\dot{\gamma}^b}. \tag{8}$$

The total stress of the mechanical analogue in Fig. 10(a) is given by the sum of the solvent, hydrodynamic, and viscoelastic stresses. Each component is subjected to the same strain and strain rate and therefore the stress and apparent viscosity of the suspension is given by

$$\sigma = \eta_s\dot{\gamma} + \eta_h\dot{\gamma} + \sigma_c, \tag{9}$$

$$\eta = \eta_s + \eta_h + \frac{\sigma_c}{\dot{\gamma}} = \eta_s + A\varepsilon_{ss} + B\varepsilon_{ss}\dot{\gamma}. \tag{10}$$

2. Step rate

The experimental data plotted in were obtained by imposing a step reduction in shear rate at $t = 0$ from 10 to 0.5 s^{-1}. For $t \geq 0$, $\varepsilon(t)$ was calculated using Eq. (11) which was obtained by integrating Eq. (5)

$$\varepsilon = \frac{V_c - (V_c - \varepsilon_{10}[V_c + V_d])\exp(-[V_c + V_d]t)}{V_c + V_d}, \tag{11}$$

where ε_{10} is the steady state value of ε at 10 s^{-1} and V_c and V_d were calculated with $\dot{\gamma} = 0.5\ s^{-1}$.

At constant shear rate, the solvent and hydrodynamic stress components are given by $\sigma_s = \eta_s\dot{\gamma}$ and $\sigma_h = \eta_h\dot{\gamma}$, respectively. The stress in the viscoelastic component, σ_e, is governed by Eq. (12), which contains additional terms to the standard Maxwell model as ε, and therefore the spring constant g and relaxation time λ vary with time

$$\dot{\gamma} = \frac{\sigma_e(t)}{\lambda(t)g(t)} + \frac{1}{g(t)}\frac{d\sigma_e(t)}{dt} - \frac{\sigma_e(t)}{\left(g(t)\right)^2}\cdot\frac{dg(t)}{dt} \quad \text{for} \quad \sigma_e < \sigma_c, \tag{12}$$

$g = C\varepsilon$ and $\lambda = D\varepsilon$ meaning that Eq. (12) can be rearranged to give

$$C\varepsilon\dot{\gamma} = \sigma_e\left(\frac{1}{D\varepsilon} - \frac{1}{\varepsilon}\cdot\frac{d\varepsilon}{dt}\right) + \frac{d\sigma_e}{dt}. \tag{13}$$

Downloaded 29 Nov 2012 to 81.132.17.87. Redistribution subject to SOR license or copyright; see http://www.journalofrheology.org/masthead

Equation (12) was solved numerically using the second order Runge-Kutta method with a step size of 0.01 s for $\sigma_e < \sigma_c$ otherwise $\sigma_e = \sigma_c$. The total stress in the suspension, σ, was calculated as the sum of σ_s, σ_h, and σ_e.

3. LVE

During the oscillatory LVE experiments, the suspensions were subjected to small deformations which were not thought to significantly affect ε. However, as G' was observed to increase with time following preshear (Fig. 9), it was assumed that the ε recovery in the absence of shear was still significant during the LVE experiments. $d\varepsilon/dt$ was then given by

$$\frac{d\varepsilon}{dt} = k_2(1-\varepsilon). \tag{14}$$

G' and G'' were given by Eqs. (15) and (16) which allowed for the variation in ε, and therefore g and λ, with time. During the fitting process, the condition that $\tau_c \geq G'$ was imposed to ensure that the slider was inactive throughout the LVE experiments

$$G' = \frac{C\varepsilon\beta\omega^2}{1+\omega^2\beta^2}, \tag{15}$$

$$G'' = (\eta_s + A\varepsilon)\omega + \frac{C\varepsilon\beta\omega}{1+\omega^2\beta^2}, \tag{16}$$

where $\beta = \left((1/D\varepsilon) - (k_2(1-\varepsilon)/\varepsilon)\right)^{-1}$.

D. Matching model and experimental data

1. Parameter estimation by minimization of errors

For each of the different forms of the model, the model parameters were chosen such that the sum of the errors between the model prediction and the experimental data (calculated using Eq. (17) for an experimentally recorded value y_{data}) were minimized. The difference in the logarithms of the experimental and model values was used as the data often spanned many decades and it was desirable that the differences between large and small data values were suppressed

$$y_{error} = (\log y_{data} - \log y_{model})^2. \tag{17}$$

The model was fitted simultaneously to data from many different rheological experiments. The number of data points varied between the experiments meaning that the total error from each experiment was weighted by a scale factor which was inversely proportional to the number of data points. The large number of model parameters and the ill-posed nature of the fitting process meant that there were many possible combinations of parameters which could result in local minima of the total error. To ensure that the final parameter values were meaningful, initial estimates were made for some parameters which were based on the experimental data as shown in Table II.

Since the model was fit to data from CB and MWNT suspensions of varying concentration, it was assumed that the parameters in the kinetic equation for ε [Eq. (5)] were independent of concentration as they relate only to the applied shear rate, and hence values of the parameters k_1, k_2, k_3, a, and b were chosen which minimized the error across all

Downloaded 29 Nov 2012 to 81.132.17.87. Redistribution subject to SOR license or copyright; see http://www.journalofrheology.org/masthead

TABLE II. Initial estimate for model parameters based on experimental data.

Parameter	Initial estimate for parameter based on experimental data
A	η(Suspension at 0.1 s^{-1}) − η(Epoxy resin)
B	σ at 0.01 s following cessation of shear at 0.5 s^{-1} at 0 s
C	G' at 100 rad s^{-1} following preshear at 0.5 s^{-1}

the CB or CNT concentrations. The number fraction of aggregated particles within a dispersion is given by ε, but the average size of the aggregates will depend on both ε and the concentration of the dispersion. Micrographs and rheological data indicate that the model parameters η_h, g, λ, and σ_c should depend on the average size of the aggregates. Therefore, it was decided to give A, B, C, and D power law dependence on concentration and the parameters within the power law relationships were chosen to minimize the error across all the CB or CNT concentrations.

2. "Best fit" parameter values

The structure-dependent hybrid Maxwell-Voigt phenomenological model with yield stress was fitted to rheological data from 1–6 wt. % CB dispersions and 0.2–0.6 wt. % MWNT suspensions. The "best fit" values of the fitting parameters are presented in Table III.

The model parameters are of the same order of magnitude for the CB and CNT suspensions which mirrors the similarities in their rheological behavior. Nevertheless, the concentration range for the CB dispersions is 1–10 wt. % CB compared to 0.1–1 wt. % MWNTs for the CNT suspensions. The parameters A, B, and C are strongly dependent on filler particle concentration indicating that σ_h, σ_c, and g are strongly influenced by aggregate size.

3. Steady shear rheology

The fit between the model and the experimental data for the apparent viscosity as a function of shear rate is shown in Fig. 11. The model has correctly predicted the shear thinning characteristic of the suspensions but it has over predicted the variation of η with $\dot{\gamma}$ at low shear. This is due to the presence of the slider yield stress in the mechanical analogue as the $\tau_c/\dot{\gamma}$ term in Eq. (10) becomes more significant at low shear.

TABLE III. Model parameters for the single Maxwell mode structure-dependent hybrid model with yield stress fitted to data from 1–6 wt. % CB dispersions and 0.2–0.6 wt. % MWNT suspensions. Φ refers to the wt. % of filler.

Model parameter (units)	Value for CB suspensions	Value for MWNT suspensions
k_1 (s^{a-1})	0.829	0.900
a (—)	0.0481	0.145
k_2 (s^{-1})	1.48×10^{-4}	2.54×10^{-4}
k_3 (s^{b-1})	4.55	1.595
b (—)	0.637	0.788
A (Pa s)	$1.25\Phi^{2.8}$	$407\Phi^{3.1}$
B (Pa)	$0.123\Phi^{3.6}$	$142\Phi^{3.9}$
C (Pa)	$4.94\Phi^{3.8}$	$54\,200\Phi^{3.8}$
D (s)	$21.0\Phi^{1.6}$	$336\Phi^{1.6}$

Downloaded 29 Nov 2012 to 81.132.17.87. Redistribution subject to SOR license or copyright; see http://www.journalofrheology.org/masthead

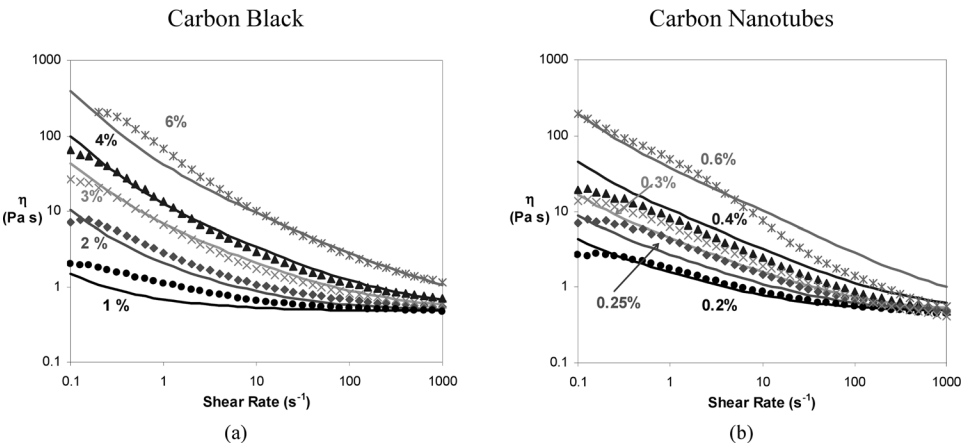

FIG. 11. Model fit (solid line) to the experimental apparent viscosity data (points) as a function of shear rate for (a) CB dispersions and (b) CNT suspensions. The model parameters were as shown in Table III.

The structure-dependent hybrid model is not the only model that could be used to describe the shear thinning behavior seen for the CB and CNT suspensions, as both the Cross model and Carreau equation will predict a similar characteristic. However, the structure-dependent hybrid model is unusual in being able to fit both linear and nonlinear viscoelastic data and steady shear data.

4. Step rate experiments

The model fit to the stress data from the 4 wt. % CB and 0.4 wt. % MWNT suspensions upon a step reduction in shear rate from 10 to 0.5 s^{-1} is shown in Fig. 12. For both the suspensions, the model correctly predicts that the stress drops rapidly with the reduction in shear rate before increasing to the new steady state value. Nevertheless, the kinetic of the stress change predicted by the model, both for the drop in σ at $t = 0$ s and the thixotropic stress increase, is much faster than was observed experimentally.

5. Oscillatory LVE

The model fit to the G' and G'' frequency sweep data for the CB and MWNT suspensions after preshear at 1 s^{-1} is shown in Fig. 13. For the CB dispersions, the model fit to the G' data improves with increasing CB concentration as G' shows less variation with ω at high frequency, as predicted by the viscoelastic Maxwell element in the model. The same is true for the high concentration MWNT suspension data, although the model predicts a much larger G' value for the 0.6 wt. % MWNTs than was observed experimentally.

The model predicts a maximum and minimum in G'' at low frequency, not seen in the data, which arises from combining G'' as predicted by the viscoelastic Maxwell element with the linear dependence of G'' on ω as predicted for the solvent and hydrodynamic parts of the model. The fit between the model and the G'' data is therefore best when the elasticity of the suspensions is small and G'' shows a steady increase with frequency, as is the case for the low concentration CB and MWNT suspensions.

The variation of G' and G'' with preshear as predicted by the model is demonstrated for 4 wt. % CB and 0.4 wt. % MWNTs in Fig. 14. The model fits the G' data for both suspensions after 1 s^{-1} preshear well and correctly predicts the decrease seen in G' and G'' with increasing preshear rate. However, as with the low concentration suspensions in Fig. 13, the model is unable to predict the steady increase in G' with ω observed in the data

Downloaded 29 Nov 2012 to 81.132.17.87. Redistribution subject to SOR license or copyright; see http://www.journalofrheology.org/masthead

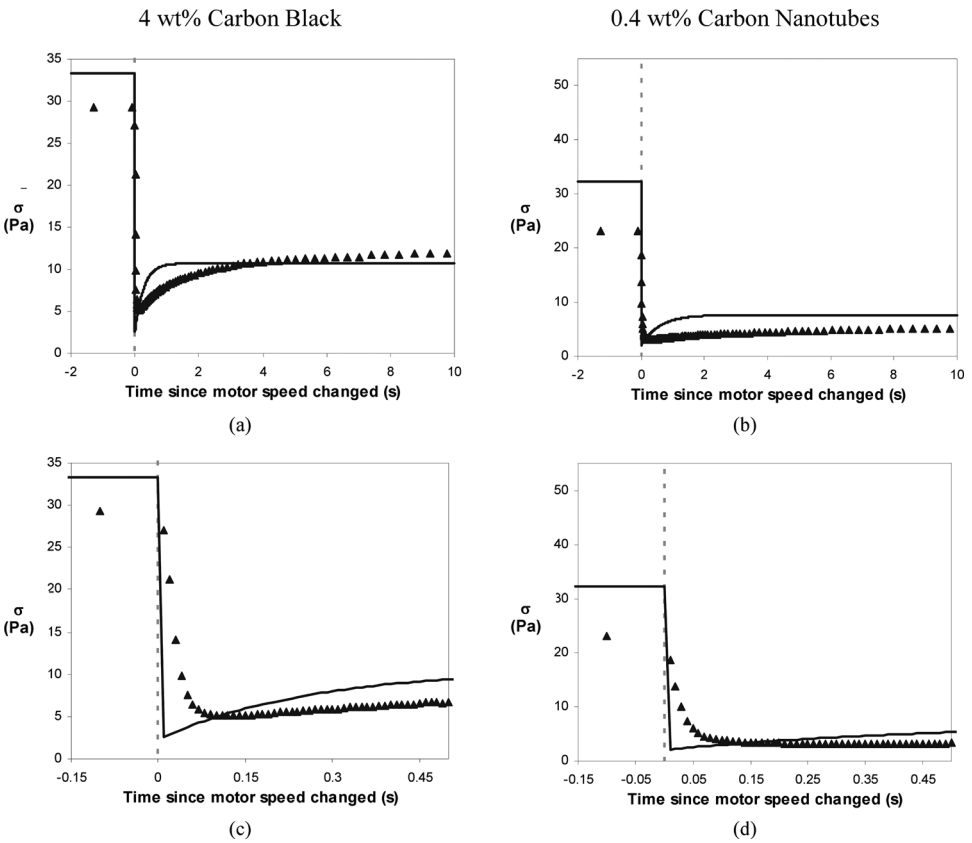

FIG. 12. Experimental stress data (points) and model fit (lines) for a step reduction in shear rate from 10 to $0.5\,s^{-1}$ at zero time: (a) 4 wt. % CB and (b) 0.4 wt. % CNT. The model predicts a much faster kinetic for stress change than was observed experimentally, as can be seen more clearly on a larger scale: (c) 4 wt. % CB and (d) 0.4 wt. % CNT. Table III shows the model parameters used in the calculations.

above ~ 0.2 rad s^{-1}, which is more prominent after high shear. The model also predicts a larger G' increase at low ω than was observed experimentally after preshear at 10 and $100\,s^{-1}$, which is an indication that the model λ values under these conditions are too low.

6. LVE recovery

Including the recovery term in the kinetic equation for ε allows G' to increase following preshear in a manner similar to the experimental data, as shown in Fig. 15 for the 4 wt. % CB and 0.4 wt. % MWNT suspensions. The model values of G' and G'' do not match the actual values at all preshear rates as the model fitting parameters are also heavily influenced by the LVE frequency sweep data in Fig. 14. The shape of the G' recovery predicted by the model differs to that of the data as the model does not capture the initial fast increase in G'.

For each of the different shear environments shown in Figs. 11–15, the actual fit between the model and the data is relatively poor, especially given the large number of parameters in the model. However, the intended scope of this model was to take a conceptually simple mechanical analogue and apply it in a larger number of different shear environments for both CB and MWNT suspensions, over a range of concentrations.

Downloaded 29 Nov 2012 to 81.132.17.87. Redistribution subject to SOR license or copyright; see http://www.journalofrheology.org/masthead

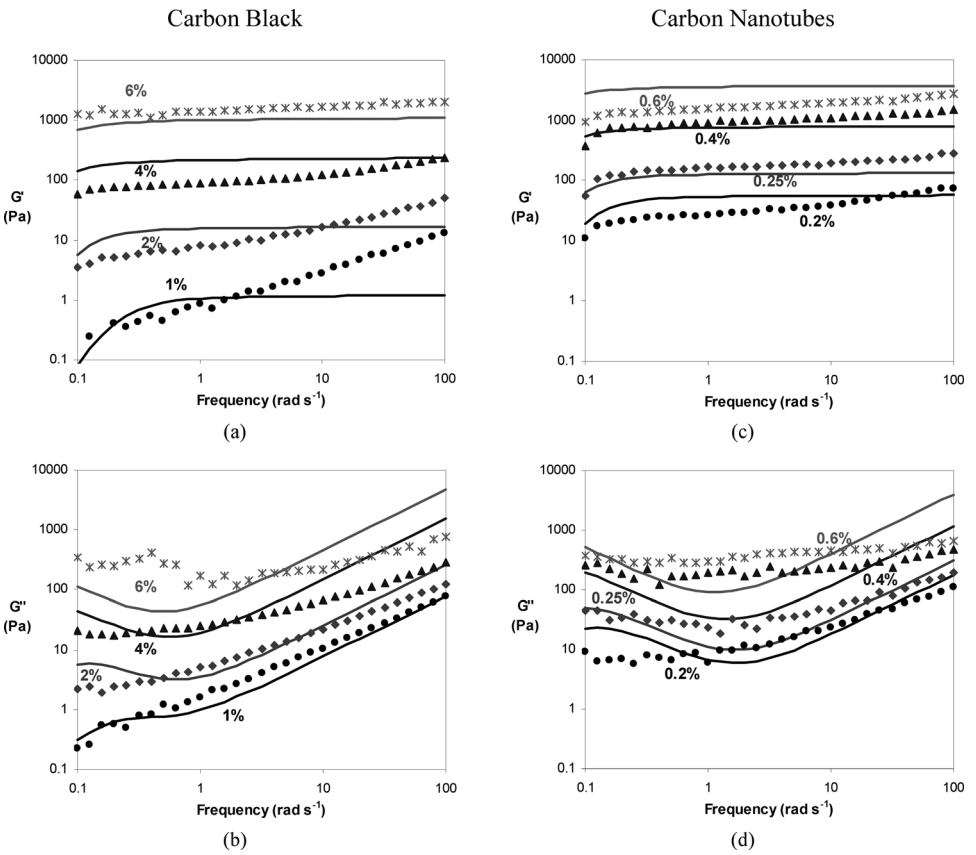

FIG. 13. Experimental data (points) and model fit (lines) for G' and G'' after preshear $1\,s^{-1}$ for 5 min: CB dispersions (a) G', (b) G''; CNT suspensions (c) G', (d) G''. Table III shows the model parameters used in the calculations.

Hence, the model has not been optimally fit to each set of experimental data but over the entire range of experiments which has meant that frequently the quality of the fit has not been that good. Nevertheless, in each case, the model has correctly predicted the trends observed experimentally over increasing filler concentration and increasing (pre)shear rate. This demonstrates the importance of aggregation, on which the model is based, on the rheological behavior of both CB and MWNT dispersions.

V. DISCUSSION

A systematic comparison of the rheological behavior of CB- and MWNT-epoxy suspensions has been carried out. Optical micrographs have shown that the structures formed by the CB and MWNT particles in the quiescent state are significantly different on the micrometer scale, with the CNTs forming structures with much larger aspect ratios than the isotropic CB particles (Fig. 1). However, despite their structural differences, the rheology of 0%–6% CB and 0%–0.6% MWNT suspensions was found to be remarkably similar which was reflected in the similar "best fit" model parameters shown in Table III. The most significant difference between the behavior of the CB and CNT dispersions was the filler concentration required to obtain the same rheological response. For

Downloaded 29 Nov 2012 to 81.132.17.87. Redistribution subject to SOR license or copyright; see http://www.journalofrheology.org/masthead

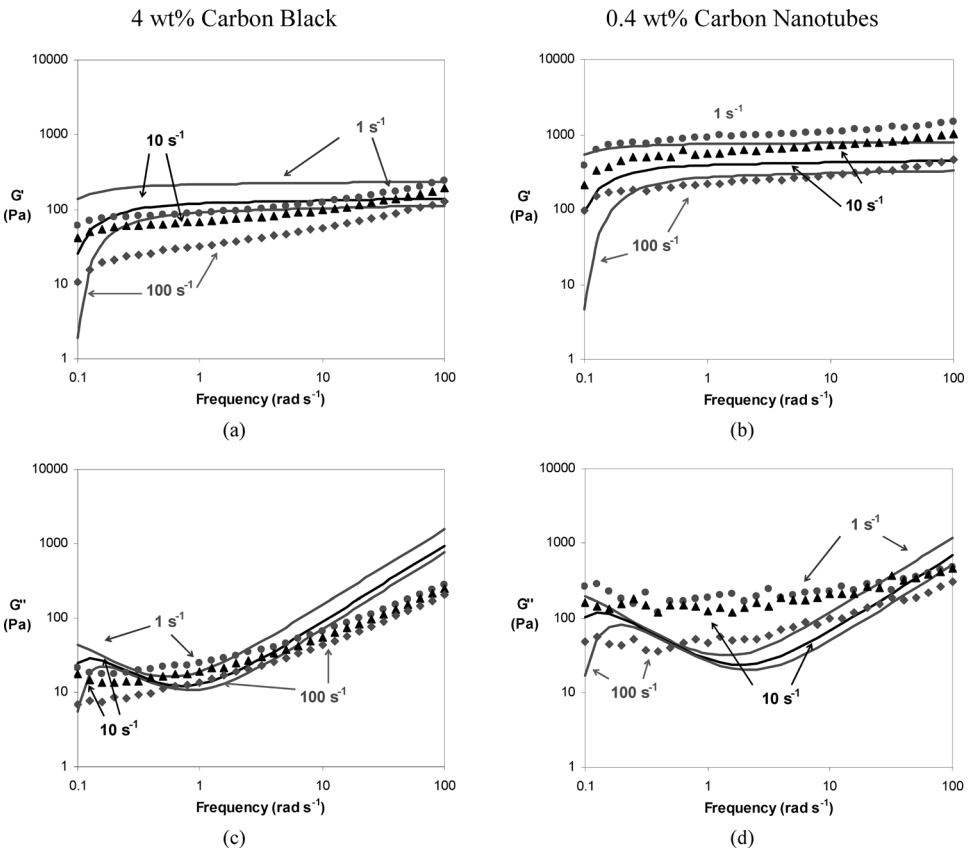

FIG. 14. Experimental data (points) and model fit (lines) for G' and G'' after preshear $1\,s^{-1}$ for 5 min, $10\,s^{-1}$ for 1 min, and $100\,s^{-1}$ for 1 min: 4 wt. % CB (a) G', (b) G''; 0.4 wt. % CNT (c) G', (d) G''. Table III shows the model parameters used in the calculations.

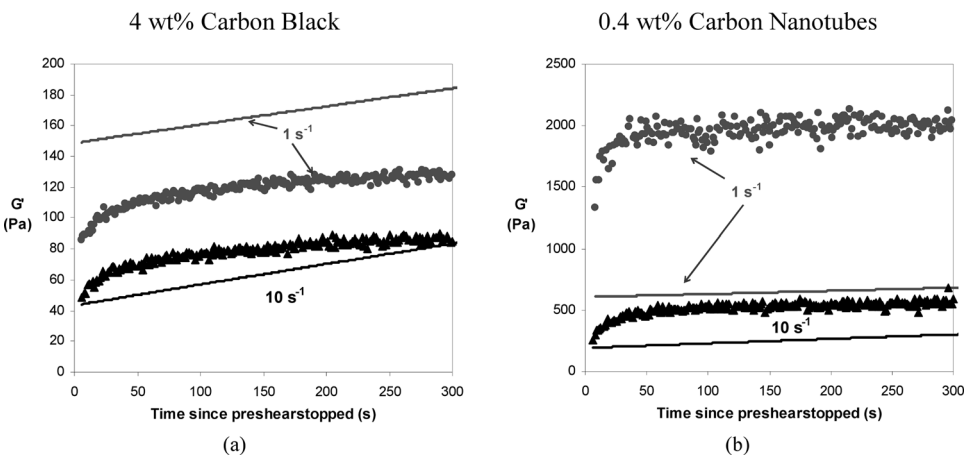

FIG. 15. Experimental data (points) and model fit (lines) for G' recovery with time following preshear at $1\,s^{-1}$ for 5 min or $10\,s^{-1}$ for 1 min: (a) 4 wt. % CB and (b) 0.4 wt. % MWNT. Readings were taken at $10\,rad\,s^{-1}$, 0.1% strain. Table III shows the model parameters used in the calculations.

Downloaded 29 Nov 2012 to 81.132.17.87. Redistribution subject to SOR license or copyright; see http://www.journalofrheology.org/masthead

example, as shown in Fig. 4, the shear dependent apparent viscosity of the 1 and 2 wt. % CB dispersions was almost identical to the 0.2 and 0.25 wt. % MWNT dispersions. The factor of ten difference in concentration was also seen when considering the rheological percolation threshold, assumed to be the filler content required to obtain a low shear plateau in G', which was found to be ~3 wt. % CB compared to ~0.25 wt. % MWNTs, as shown in Fig. 7.

Optical micrographs of CB and MWNT suspensions following shear at different rates (Fig. 3) have shown that filler particle aggregation at low shear and aggregate destruction at high shear was a process common to both CB and MWNTs. The apparent viscosity and elasticity of the suspensions were clearly related to the average size of the aggregates as η decreased with increasing shear (Fig. 4) and G' decreased following shear at a higher rate (Fig. 8). Hence, a phenomenological rheological model with parameters dependent on the state of aggregation within the suspensions was able to capture the key features of the CB and MWNT suspensions such as decreasing elasticity with increased preshear rate and thixotropic stress recovery equally well (Figs. 11–15).

The enhanced steady shear apparent viscosity of CB dispersions at low shear has been linked to the increased viscous drag between larger aggregates [see for example Dullaert and Mewis (2006)] and, given their similar rheology, it appears that an analogous effect occurs within the flocculating MWNT suspensions. The suspension viscosity therefore depends on the size of the CB or CNT aggregates and the difference in filler particle concentration required to obtain the same viscosity can be explained by considering the packing density of CB or CNTs within the aggregates. Quemada (1998) has extended the relationship proposed by Kreiger and Dougherty (1959) for the relative viscosity of a suspension of hard spheres [Eq. (18)] to a suspension of flocculating particles [Eq. (19)]

$$\eta_r = \left(1 - \frac{\phi}{\phi_0}\right)^{-q}, \tag{18}$$

$$\eta_r = \left(1 - \frac{\phi}{\varphi\phi_m}\right)^{-q}. \tag{19}$$

In Eq. (18) ϕ is the volume fraction of filler particles, ϕ_0 is the maximum volume fraction of particles, and q is the product of $[\eta]$, the intrinsic viscosity of suspended particles, and ϕ_0. For spheres in the dilute regime, the intrinsic viscosity given by the Einstein Equation is 2.5. Many expressions exist for the viscosity of suspensions of rods [see for example Petrie (1999)] that in general result in intrinsic viscosities much greater than 2.5.

In Eq. (19), developed by Quemada (1998), the particles are assumed to form spherical aggregates called "structural units" which are all the same size. An allowance has been made for fluid trapped within the aggregates through the use of φ, denoted "compactness," which is given by Eq. (20). ϕ_m is the maximum packing of the structural units

$$\varphi = \frac{\text{volume of filler particles in agglomerate}}{\text{total volume of agglomerate}}. \tag{20}$$

The model propose by Quemada (1998) is clearly an oversimplification for the CB and CNT suspensions but the argument that less compact structural units have the same effect on viscosity as aggregates with the same total volume still applies. The structure of the MWNTs in suspension, as long and often bent fibres, meant that they could not pack as

Downloaded 29 Nov 2012 to 81.132.17.87. Redistribution subject to SOR license or copyright; see http://www.journalofrheology.org/masthead

easily within the aggregates as the approximately spherical CB particles. This can be appreciated from Figs. 3(a) and 3(d) in which the aggregates formed by the CB particles at $0.5\,s^{-1}$ appear opaque whereas clear gaps can be seen between the MWNT particles although the MWNTs have formed an aggregate of a similar size to the CB aggregate. Hence, a significantly higher loading of CB is required to obtain the same viscosity enhancement as a MWNT suspension.

With regards to the suspensions' elasticity, a distinction should be made between unsheared dispersions in the quiescent state and suspensions which have been subjected to preshear. In the absence of shear, Fig. 2 demonstrates that the fibre-like nature of the MWNT structures promotes the formation of a continuous filler particle network at relatively low concentrations. By contrast, the isotropic CB particles form CB aggregates in the quiescent state which grow in size as the filler particle concentration is increased. Hence the percolation threshold of the CNT suspensions is significantly lower than for the CB dispersions as percolation for the CB suspensions can only occur once the CB aggregates are large enough to impinge on each other, whereas the MWNT structures can form a continuous network without significant aggregate formation.

Once the suspensions have been subjected to preshear, the filler particles form aggregates, the size of which is governed by the filler particle concentration and shear rate. As discussed by Hobbie and Fry (2007) and Shoukens and Mewis (1978), it is thought that the suspensions' elasticity arises from interactions between the filler particles inside the aggregates and between the aggregates themselves. The relationship between aggregate size and suspension elasticity can be appreciated from the "best fit" values of the structure-dependent model parameters. In particular, the model has been devised such that the extent of aggregation, represented by ε, is the same for each CB or CNT suspension at a given shear rate and therefore the actual size of the aggregates is dependent on the suspension concentration. As shown in Table III, both B and C (and therefore σ_c and g) are strongly dependent on concentration for the CB and CNT dispersions. Hence, the yield stress and elasticity of the suspensions increases as the aggregate size increases. A low concentration suspension may contain filler particles which are nearly all aggregates ($\varepsilon \approx 1$), but if there is significant space between the aggregates, then the interactions between them are relatively weak such that the limiting stress (σ_c) and stiffness (g) of the viscoelastic network are low. For the same value of ε, a more concentrated dispersion may contain a continuous aggregate meaning both σ_c and g are significantly larger as the forces imposed on the sample are transmitted throughout the entire aggregate network.

Although the structure-dependent model presented in Fig. 10 has predicted the key features of the CB and CNT suspension rheology, the model has been unable to capture some of the more subtle rheological behavior such as G' increasing with frequency at large values of ω. However, it is well established that data matching with mechanical models can be improved by introducing multimodes of elements which introduces a spectrum of relaxation processes within the model [Baumgaertel and Winter (1989); Mackley *et al*. (1994)]. Given the complex nature of the CB and CNT suspensions, there are likely to be multiple relaxation modes active within the suspensions; for example, there will be a difference between the viscoelastic interactions between particles within an aggregate and between the aggregates themselves. Nevertheless, the single viscoelastic Maxwell element model is relatively simple to work with and is able to give a qualitative understanding of the suspensions. The model fits the data best when the filler particle aggregates are large (i.e., at high concentration—Fig. 13—and after low preshear—Fig. 14) as the aggregates are more likely to extend across the suspension, meaning that the viscoelasticity of the dispersion is dominated by the interactions between particles within the aggregates.

Downloaded 29 Nov 2012 to 81.132.17.87. Redistribution subject to SOR license or copyright; see http://www.journalofrheology.org/masthead

VI. CONCLUSIONS

A systematic study of the effect of flow on CB- and MWNT-epoxy suspensions has been performed, focussing on the suspensions' microstructure and rheology. Despite the differences between the microstructures of the CB and MWNT entities, the rheological behavior of the suspensions was found to be remarkably similar although approximately ten times as much CB was required to obtain the same response as the MWNT dispersions. Optical microscopy of suspensions following shear at different rates revealed that both the CB and MWNTs formed large aggregates at low shear which were broken down at high shear. Hence, a relatively simple structure-dependent mechanical analogue model was developed, which separated the hydrodynamic and viscoelastic effects of the filler. In order to achieve self consistency between steady shear and LVE behavior, a slider yield stress had also to be introduced into the model. The model showed a reasonably good fit to both the CB and MWNT data, with similar "best fit" parameters for both systems, which demonstrated the similarity between the CB and MWNT suspensions' rheology. Based on these findings, it is clear that for these two different suspensions at least, there is a universal rheological response for fluids such as CB and MWNT dispersions and that the rheology is strongly influenced by aggregate size with the differences in filler particle nanostructure affecting the percolation critical concentration behavior of the suspensions.

ACKNOWLEDGMENTS

The authors would like to thank Dr. Simon Butler for assistance with rheological measurements. K.M.Y. would like to thank EPSRC for financial support through a Doctoral Training award.

References

Ahir, S. V., Y. Y. Huang, and E. M. Terentjev, "Polymers with aligned carbon nanotubes: Active composite materials," Polymer **49**(18), 3841–3854 (2008).

Alig, I., D. Lellinger, and T. Skipa, "Influence of thermo-rheological history on electrical and rheological properties of polymer-carbon nanotube composites," in *Polymer-Carbon Nanotube Composites. Preparation, Properties and Applications*, edited by T. McNally and P. Pötschke (Woodhead, Cambridge, UK, 2011), pp. 295–328.

Alig, I., T. Skipa, D. Lellinger, and P. Pötschke, "Destruction and formation of a carbon nanotube network in polymer melts: Rheology and conductivity spectroscopy," Polymer **49**(16), 3524–3532 (2008).

Aoki, Y., A. Hatano, and H. Watanabe, "Rheology of carbon black suspensions. I. Three types of viscoelastic behavior," Rheol. Acta **42**, 209–216 (2003).

Barrie, C. L., P. C. Griffiths, R. J. Abbott, I. Grillo, E. Kudryashov, and C. Smyth, "Rheology of aqueous carbon black dispersions," J. Colloid Interface Sci. **272**(1), 210–217 (2004).

Baumgaertel, M., and H. H. Winter, "Determination of discrete relaxation and retardation time spectra from dynamic mechanical data," Rheol. Acta **28**(6), 511–519 (1989).

Bigg, D. M., "An investigation of the effect of carbon black structure, polymer morphology and processing history on the electrical conductivity of carbon-black-filled thermoplastics," J. Rheol. **28**(5), 501–516 (1984).

Bose, S., R. A. Khare, and P. Moldenaers, "Assessing the strengths and weaknesses of various types of pre-treatments of carbon nanotubes on the properties of polymer/carbon nanotubes composites: A critical review," Polymer **51**(5), 975–993 (2010).

Bower, C., M. R. Mackley, B. A. S. Smeulders, D. Barker, and J. Hayes, "The rheology, processing and microstructure of complex fluids," in *Modern Aspects of Colloidal Dispersions*, edited by R. H. Ottewill and A. R. Rennie (Kluwer Academic, Dordrecht, The Netherlands, 1998), pp. 279–289.

Downloaded 29 Nov 2012 to 81.132.17.87. Redistribution subject to SOR license or copyright; see http://www.journalofrheology.org/masthead

Cabot Corporation, "Vulcan XC conductive blacks for premium performance in electrostatic discharge (ESD) applications," Product promotional material, 2008.

Carvalho, M., M. Padmanabhan, and C. W. Macosko, "Single-point correction for parallel disks rheometry," J. Rheol. **38**(6), 1925–1936 (1994).

Chapartegui, M., N. Markaide, S. Florez, C. Elizetxea, M. Fernandez, and A. Santamaría, "Specific rheological and electrical features of carbon nanotube dispersions in an epoxy matrix," Comp. Sci. Tech. **70**(5), 879–884 (2010).

Coussot, P., and A. I. Leonov, "Rheology molecular of concentrated weight matrix dispersed systems in a low," J. Non-Newtonian Fluid Mech. **46**, 179–211 (1993).

Du, F., R. C. Scogna, W. Zhou, S. Brand, J. E. Fischer, and K. I. Winey, "Nanotube networks in polymer nanocomposites: Rheology and electrical conductivity," Macromol. **37**(24), 9048–9055 (2004).

Dullaert, K., and J. Mewis, "A structural kinetics model for thixotropy," J. Non-Newtonian Fluid Mech. **139**(1–2), 21–30 (2006).

Fischer, J. E., H. Dai, A. Thess, R. Lee, N. M. Hanjani, D. L. Dehaas, and R. E. Smalley, "Metallic resistivity in crystalline ropes of single-wall carbon nanotubes," Phys. Rev. B **55**(8), R4921–R4924 (1997).

Kirk-Othmer Encyclopedia of Chemical Technology, 3rd ed., edited by M. Grayson (Wiley-Interscience, USA, 1978), Vol. 4, pp. 631–666.

Hobbie, E. K., and D. J. Fry, "Rheology of concentrated carbon nanotube suspensions," J. Chem. Phys. **126**(12), 124907 (2007).

Hu, G., C. Zhao, S. Zhang, M. Yang, and Z. Wang, "Low percolation thresholds of electrical conductivity and rheology in poly(ethylene terephtalate) through the networks of multi-walled carbon nanotubes," Polymer **47**(1), 480–488 (2006).

Hu, Y., H. Zhang, B. Zhou, and C. Cai, "Bimetallic Pt-Au nanocatalysts electrochemically deposited on graphene and their electrocatalytic characteristics towards oxygen reduction and methanol oxidation," Phys. Chem. Chem. Phys. **13**, 4083–4094 (2011).

Iijima, S., "Helical microtubules of graphitic carbon," Nature **354**, 56–58 (1991).

Jin, L., C. Bower, and O. Zhou, "Alignment of carbon nanotubes in a polymer matrix by mechanical stretching," Appl. Phys. Lett. **73**(9), 1197 (1998).

Kawaguchi, M., M. Okuno, and T. Kato, "Rheological properties of carbon black suspensions in a silicone oil," Langmuir **17**(20), 6041–6044 (2001).

Khalkhal, F., P. J. Carreau, and G. Ausias, "Effect of flow history on linear viscoelastic properties and the evolution of the structure of multiwalled carbon nanotube suspensions in an epoxy," J. Rheol. **55**(1), 153 (2011).

Kim, P., L. Shi, A. Majumdar, and P. McEuen, "Thermal transport measurements of individual multiwalled nanotubes," Phys. Rev. Lett. **87**(21), 19–22 (2001).

Kinloch, I. A., S. A. Roberts, and A. H. Windle, "A rheological study of concentrated aqueous nanotube dispersions," Polymer **43**, 7483–7491 (2002).

Krishnan, A., E. Dujardin, T. Ebbesen, P. Yianilos, and M. Treacy, "Young's modulus of single-walled nanotubes," Phys. Rev. B **58**(20), 14013–14019 (1998).

Lin-Gibson, S., J. Pathak, E. Grulke, H. Wang, and E. Hobbie, "Elastic flow instability in nanotube suspensions," Phys. Rev. Lett. **92**(4), 1–4 (2004).

Lisunova, M. O., N. I. Lebovka, O. V. Melezhyk, and Y. P. Boiko, "Stability of the aqueous suspensions of nanotubes in the presence of nonionic surfactant," J. Colloid Interface Sci. **299**(2), 740–746 (2006).

Lobe, V. M., and J. L. White, "An experimental study of the influence of carbon black on the rheological properties of a polystyrene melt," Polym. Eng. Sci. **19**(9), 617–624 (1979).

Ma, A. W. K., K. Yearsley, F. Chinesta, and M. Mackley, "A review of the microstructure and rheology of carbon nanotube suspensions," Proc. Inst. Mech. Eng., Part N: J. Nanoeng. Nanosyst. **222**(34), 71–94 (2008b).

Ma, A. W. K., M. R. Mackley, and F. Chinesta, "The microstructure and rheology of carbon nanotube suspensions," Int. J. Mater. Form. **1**(2), 75–81 (2008a).

Mackley, M., R. Marshall, J. Smeulders, and F. Zhao, "The rheological characterization of polymeric and colloidal fluids," Chem. Eng. Sci. **49**(16), 2551–2565 (1994).

Mackley, M. R., S. Wannaborworn, P. Gao, and F. Zhao, "The optical microscopy of sheared liquids using a newly developed optical stage," J. Microscopy Analysis **69**, 25–27 (1999).

Downloaded 29 Nov 2012 to 81.132.17.87. Redistribution subject to SOR license or copyright; see http://www.journalofrheology.org/masthead

Mewis, J., and G. Schoukens, "Mechanical spectroscopy of colloidal dispersions," Faraday Discuss. **65**, 58–64 (1978).

Mewis, J., and N. J. Wagner, "Thixotropy," Adv. Colloid Interface Sci. **147–148**, 214–227 (2009).

Mewis, J., and N. J. Wagner, "Short course in suspension rheology," in Society of Rheology 82nd Annual Meeting, Santa Fe, NM, 2010.

Mobuchon, C., P. J. Carreau, and M. C. Heuzey, "Structural analysis of non-aqueous layered silicate suspensions subjected to shear flow," J. Rheol. **53**, 1025–1049 (2009).

Mujumdar, A., A. N. Beris, and A. B. Metzner, "Transient phenomena in thixotropic systems," J. Non-Newtonian Fluid Mech. **102**(2), 157–178 (2002).

Nobile, M. R., "Rheology of polymer-carbon nanotube composite melts," in *Polymer-Carbon Nanotube Composites. Preparation, Properties and Applications*, edited by T. McNally and P. Pötschke (Woodhead, Cambridge, UK, 2011), pp. 428–481.

Osuji, C. O., and D. A. Weitz, "Highly anisotropic vorticity aligned structures in a shear thickening attractive colloidal system," Soft Matter **4**(7), 1388 (2008).

Park, S. J., M. S. Cho, S. T. Lim, H. J. Choi, and M. S. Jhon, "Synthesis and dispersion characteristics of multiwalled carbon nanotube composites with poly(methyl methacrylate) prepared by in-situ bulk polymerisation," Macromol. Rapid Commun. **24**(18), 1070–1073 (2003).

Park, O., M. T. Jeevananda, N. Kim, S. Kim, and J. Lee, "Effects of surface modification on the dispersion and electrical conductivity of carbon nanotube/polyaniline composites," Scripta Materialia **60**(7), 551–554 (2009).

Petrie, C. J. S., "The rheology of fibre suspensions," J. Non-Newtonian Fluid Mech. **87**, 369–402 (1999).

Pujari, S., S. Rahatekar, J. W. Gilman, K. K. Koziol, A. H. Windle, and W. R. Burghardt, "Shear-induced anisotropy of concentrated multiwalled carbon nanotube suspensions using x-ray scattering," J. Rheol. **55**(5), 1033 (2011).

Quemada, D., "Rheological modelling of complex fluids. I. The concept of effective volume fraction revisited," Eur. Phys. J.: Appl. Phys. **1**(1), 119–127 (1998).

Quemada, D., "Rheological modelling of complex fluids: IV: Thixotropic and "thixoelastic" behaviour. Start-up and stress relaxation, creep tests and hysteresis cycles," Eur. Phys. J.: Appl. Phys. **5**(2), 191–207 (1999).

Rahatekar, S. S., K. K. Koziol, S. A. Butler, J. A. Elliott, M. S. P. Shaffer, M. R. Mackley, and A. H. Windle, "Optical microstructure and viscosity enhancement for an epoxy resin matrix containing multiwall carbon nanotubes," J. Rheol. **50**(5), 599 (2006).

Sandler, J., M. S. P. Shaffer, T. Prasse, W. Bauhofer, K. Schulte, and A. H. Windle, "Development of a dispersion process for carbon nanotubes in an epoxy matrix and the resulting electrical properties," Polymer **40**(21), 5967–5971 (1999).

Schoukens, G., and J. Mewis, "Nonlinear dependent rheological structure behaviour in colloidal and shear-dispersions," J. Rheol. **22**, 381–394 (1978).

Singh, C., M. S. P. Shaffer, and A. H. Windle, "Production of controlled architectures of aligned carbon nanotubes by an injection chemical vapour deposition method," Carbon **41**(2), 359–368 (2003).

Skipa, T., D. Lellinger, W. Böhm, M. Saphiannikova, and I. Alig, "Influence of shear deformation on carbon nanotube networks in polycarbonate melts: Interplay between build-up and destruction of agglomerates," Polymer **51**(1), 201–210 (2010).

Tomantschger, K., and K. V. Kordesch, "Structural analysis of alkaline fuel cell electrodes and electrode materials," J. Power Sources **25**, 195–214 (1989).

White, J. L., and J. W. Crowder, "The influence of carbon black on the extrusion characteristics and rheological properties of elastomers: Polybutadiene and butadiene–styrene copolymer," J. Appl. Polym. Sci. **18**(4), 1013–1038 (1974).

Yearsley, K. M., "The effect of flow on carbon black and carbon nanotube suspensions," Ph.D. thesis, University of Cambridge, 2011.

Yziquel, F., P. J. Carreau, M. Moan, and P. A. Tanguy, "Rheological modeling of concentrated colloidal suspensions," J. Non-Newtonian Fluid Mech. **86**, 133–155 (1999).

Downloaded 29 Nov 2012 to 81.132.17.87. Redistribution subject to SOR license or copyright; see http://www.journalofrheology.org/masthead